

Simulation-based design and optimization of Francis turbine runners by using multiple types of metamodels

Proc IMechE Part C:
J Mechanical Engineering Science
2017, Vol. 231(8) 1427–1444
© IMechE 2016
Reprints and permissions:
sagepub.co.uk/journalsPermissions.nav
DOI: 10.1177/0954406216658078
journals.sagepub.com/home/pic



Fatma Ayancik^{1,2}, Erdem Acar¹, Kutay Celebioglu² and Selin Aradag^{1,2}

Abstract

In recent years, optimization started to become popular in several engineering disciplines such as aerospace, automotive and turbomachinery. Optimization is also a powerful tool in hydraulic turbine industry to find the best performance of turbines and their sub-elements. However, direct application of the optimization techniques in design of hydraulic turbines is impractical due to the requirement of performing computationally expensive analysis of turbines many times during optimization. Metamodels (or surrogate models) that can provide fast response predictions and mimic the behavior of nonlinear simulation models provide a remedy. In this study, simulation-based design of Francis type turbine runner is performed by following a metamodel-based optimization approach that uses multiple types of metamodels. A previously developed computational fluid dynamics-based methodology is integrated to the optimization process, and the results are compared to the results obtained from on-going computational fluid dynamics studies. The results show that, compared to the conventional methods such as computational fluid dynamics-based methods, metamodel-based optimization can shorten the design process time by a factor of 9.2. In addition, with the help of optimization, turbine performance is increased while cavitation on the turbine blades, which can be harmful for the turbine and reduce its lifespan, is reduced.

Keywords

Francis turbine, runner, metamodel, optimization, DesignXplorer, computational fluid dynamics

Date received: 29 December 2015; accepted: 13 June 2016

Introduction

Hydro power is the world's most reliable, affordable, available and sustainable energy source. It provides 19% of the planet's electricity, and it only requires flowing or fast running water to generate energy that can be captured and converted into electricity. Turbines are used for hydro power generation.¹

Francis turbines are preferred to other types because of their wide range of flow rate and head values. They are composed of five different components, amongst which the runner is the most important one because it directly affects the performance of the turbine. Runner is connected to the generator which generates electricity. The dimensions and the shape of Francis turbine runners are determined based on several objectives and constraints.² Flow in Francis turbine runners is rotational and three-dimensional; therefore, two-dimensional methods

cannot be applied.³ Computational fluid dynamics (CFD) is the most commonly used tool that makes internal flows in such complex domains predictable and it captures the flow physics which has a substantial influence on the performance of hydro turbines. In conventional CFD-based design, the designer performs runner design based on trial and error; therefore, the designer tends to stay within the bounds of successful previous studies.²

There are many considerations to be taken into account in the design procedure. Head and discharge

¹Department of Mechanical Engineering, TOBB University of Economics and Technology, Ankara, Turkey

²Hydro Energy Research Laboratory, TOBB University of Economics and Technology, Ankara, Turkey

Corresponding author:

Erdem Acar, TOBB University of Economics and Technology, Sogutozu Cad. No: 43, Sogutozu, Ankara 06560, Turkey.
Email: acar@etu.edu.tr

are the input parameters to determine the dimensions of the turbine and the general shape of the runner and its blades. Head is the difference between the upstream energy level of the fluid entering the turbine and the downstream energy level. Turbine power, turbine efficiency, head and flow coefficients are other considerations in the design process. Turbine power is the hydraulic power generated by the turbine. Efficiency is described as a ratio of the measured performance to the theoretical performance of a turbine. Head and flow coefficients are the non-dimensional parameters which express turbine characteristics. If the values are known, they are used to calculate the parameters, such as head and discharge.⁴ Cavitation is another important consideration that needs to be eliminated. It occurs at high-flow velocity regions when the local static pressure decreases below the vapor pressure.⁵ Turbine blades can get harmed and the performance of turbine may be reduced because of the bubbles.

CFD has become one of the main tools for turbo machinery applications.⁶ It provides predictable internal flows, information about flow separation, sources of loss and loss distribution in the components of turbine and also risky regions that are inclined to cavitation.⁷ The use of CFD has become more affordable at all levels of the turbine applications and their performance analyses since 1970s, using different levels of complexity and assumptions (Euler-3D, Reynolds averaged Navier–Stokes (RANS), large eddy simulations, etc.) RANS simulation is a commonly used technique for performance analyses. This is preferred because of its efficiency and speed. Therefore, Drtina and Sallaberger,⁵ Wu et al.⁸ and Nilsson and Davidson⁹ used RANS simulations in CFD with different turbulence models to design and test their studies. Another reason to choose this simulation type besides the speed and efficiency is that, it captures the secondary flows and turbulent flow in boundary layer accurately.

In this paper, CFD is used for analyzing the performance of the turbine runner. Conventional CFD-based design process is executed through trial and error; hence, designing a runner for a Francis type turbine can take several months. Also during this process, the designer is restricted to stay in the limits of previous studies. Due to these drawbacks of conventional CFD-based design, CFD-driven optimization approaches can be followed. Wu et al.⁸ used a CFD-driven optimization approach to optimize whole Francis type turbine elements and to reach the best efficiency point. Derakhshan and Mostafavi¹⁰ indicated that turbine performance depends on runner blade shapes, and he focused on the design of a small Francis turbine runner by using artificial neural networks and genetic algorithms (GAs) coupled with 3D Navier–Stokes flow. The main purpose was to improve the performance of initial geometry of the runner blade. To reduce the

computational time, Thum and Schilling¹¹ used different CFD codes such as quasi-3D-Euler, 3D-Euler and 3D Navier–Stokes codes with parameterized blade geometry. To keep the geometry invariable during the optimization process, Thum and Schilling¹¹ used B-Spline modification technique.

Another optimization approach is the integrated optimization with CFD, and Georgopoulou et al.¹² performed such kind of study by using metamodel-assisted evolutionary algorithms. One year later, Nakamura and Kurosawa¹³ performed an optimization study on turbine blades by using GA. In 2012, Enomoto et al.¹⁴ designed a turbine blade for Francis type turbine with the help of design of experiments (DoE). All analyses are performed with the help of CFD. Two years later, Kawajiri et al.¹⁵ used the same tool by using multi-objective GA (MOGA) with the same purpose which is to find the most efficient Francis turbine runner blade. However, it was shown that the use of the most accurate metamodel in optimization does not necessarily lead to the optimum solution.¹⁶ Therefore, in this study, optimization is performed with different metamodel types to obtain multiple optimum solution candidates, and the candidate with best performance is chosen to be the optimum configuration.

Problem description

Hydraulic turbine design requires searching for the proper values of design variables of runner blades to obtain desired cavitation-free shape with high efficiency by given parameters such as head, volumetric flow rate and runner rotational speed. These parameters constitute the optimization problem as objective function and constraints.

A constrained nonlinear optimization problem is stated mathematically as

$$\text{Min/Max } f_i(x), \quad i=1, 2, \dots, n_f \quad (1a)$$

$$\text{Subject to } g_j(x) \leq 0, \quad j=1, 2, \dots, n_g \quad (1b)$$

$$x \in S \quad (1c)$$

In this formulation, x is an n -dimensional vector of unknowns $x = (x_1, x_2, \dots, x_n)$ called design variables, f_i and g_j are the objective and constraints functions, respectively. Set S is a subset of n -dimensional space that defines the design space (i.e., the bounds of the design variables).^{17,18}

In this study, the design variables are the lean and metal angles for five different spans of the meridional surface. The lean and metal angles form the curvilinear shape of the blade which is crucial for optimum design (cavitation-free surface, high efficiency). Lean angle is defined by the angle “ θ ” between the blade and meridional plane. It is measured perpendicular to the stream surface, $\psi=0$. When lean angle is set up accurately,

it regulates cross flow on the runner blade to balance the pressure for potential flow.¹⁹ This means that to reduce cavitation on the blade surface, lean angle is a characteristic parameter. On the other hand, lean angle θ is dependent to metal angle “ ξ ” which constitutes the curvature of the blade. Demonstration of lean angle can be seen in Figure 1.²⁰ Also, the span distribution on meridional surface is shown in Figure 2.

In the present work, we consider two different cases for optimization. For the first case (i.e., the single objective optimization case), the objective function is the turbine efficiency that needs to be maximized. The available head, shaft power and cavitation values should satisfy the constraints. For the first optimization case, the design variables are the metal angles.

The optimization problem for the first case can be stated as

$$\text{Max } \eta(x) \tag{2a}$$

$$H_U \geq H(x) \geq H_L \tag{2b}$$

$$C(x) \geq C_{\min} \tag{2c}$$

$$SP_U \geq SP(x) \geq SP_L \tag{2d}$$

$$x \in S \tag{2e}$$

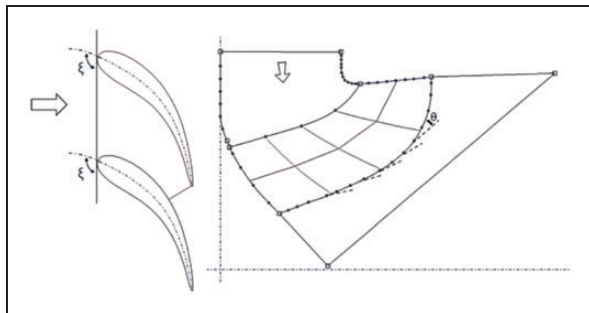


Figure 1. Lean and metal angle on turbine blade.

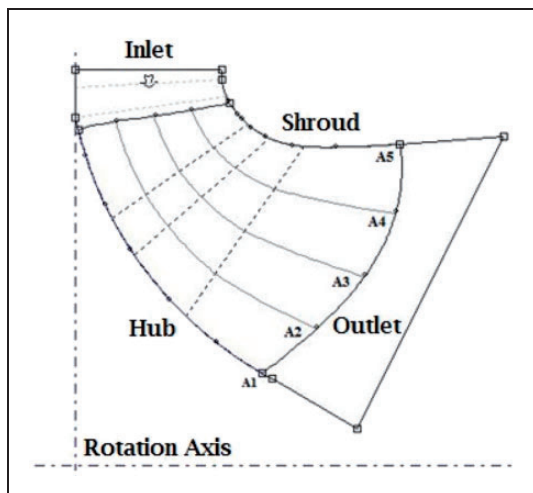


Figure 2. Span distribution on meridional surface.

Here, the first constraint restricts the head, the second constraint restricts cavitation and the third constraint restricts the shaft power. The parameters used in these constraints are given in Table 1.

Table 1. Parameters in design constraints.

H_L (m)	H_U (m)	C_{\min} (kPa)	SP_L (MW)	SP_U (MW)
44	46	-66	1.0	1.2

Table 2. Design variables and responses.

Design variables (input parameters)	Responses (output parameters)
0% Span (A_1)	Head (m)
20% Span (A_2)	Turbine power (MW)
50% Span (A_3)	Total efficiency
75% Span (A_4)	Cavitation (kPa)
100% Span (A_5)	

Table 3. Initial wide range of the design variables.

Design variable	Lower	Upper
Metal angles ($^\circ$)		
0% Span (A_1)	30	80
20% Span (A_2)	30	80
50% Span (A_3)	30	80
75% Span (A_4)	30	80
100% Span (A_5)	30	80
Lean angles ($^\circ$)		
0% Span (A_1)	-20	30
20% Span (A_2)	-20	30
50% Span (A_3)	-20	30
75% Span (A_4)	-20	30
100% Span (A_5)	-20	30

Table 4. Final values of the lower and upper bounds of the design variables.

Design variable	Lower	Upper
Metal angles ($^\circ$)		
0% Span (A_1)	67.6	77.6
20% Span (A_2)	66.0	76.0
50% Span (A_3)	65.5	75.5
75% Span (A_4)	60.5	74.1
100% Span (A_5)	59.0	72.1
Lean angles ($^\circ$)		
0% Span (A_1)	-12.0	4.0
20% Span (A_2)	-12.0	3.0
50% Span (A_3)	-9.0	5.0
75% Span (A_4)	-3.0	6.0
100% Span (A_5)	3.0	7.0

For the second case (i.e., the multi-objective optimization case), elimination of cavitation is considered so minimization of cavitation pressure becomes the other objective function. Constraints are the same except cavitation-free surface requirement. For the second optimization case, the design variables are

the lean angles. The optimization problem for the second case can be stated as

$$\text{Max } \eta(x), \quad \text{Min } C(x) \tag{3a}$$

$$H_U \geq H(x) \geq H_L \tag{3b}$$

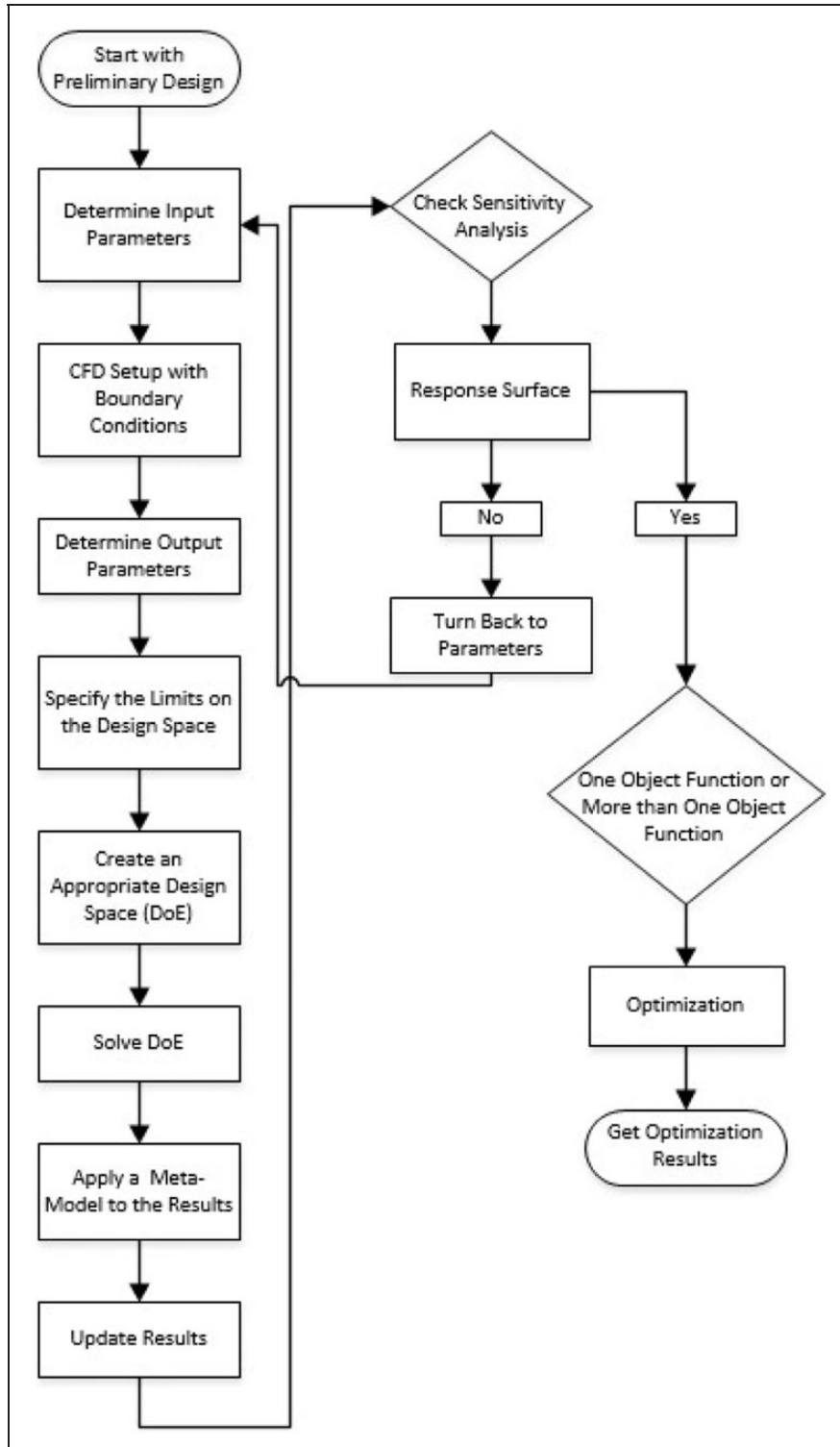


Figure 3. CFD-aided optimization procedure. CFD: computational fluid dynamics; DoE: design of experiments.

$$SPU \geq SP(x) \geq SPL \tag{3c}$$

$$x \in S \tag{3d}$$

The design variables and the responses in the optimization problems of our interest are listed in Table 2. It can be noticed that the lean and metal angles at five different span (0%, 20%, 50%, 75% and 100%) of the meridional surface are used as design variables.

To form the design space S , lower and upper bounds of the design variables need to be defined. Determination of these bounds through 3-D CFD analyses is computationally costly. Therefore, turbine runner blades are generated by using BladeGen module of Ansys²¹ without thickness, and the flow is assumed to be two dimensional to determine these bounds. The general shape of the runner and flow conditions are kept fixed. The lower and upper bounds of the angles at different spans are the same, since these preliminary analyses are based on the use of using BladeGen module without thickness. Analyses start with a wide range of the design variables (see Table 3). Notice that lower and upper bounds of the angles at different spans are taken the same as 2-D analyses that are performed to determine these bounds. For each simulation, only one parameter is changed, and the others are kept constant. This procedure is repeated for each parameter. Depending upon convergence and divergence of the results, the bounds of the design variables are narrowed or extended, and correlation between parameters are defined. The final values of the lower and upper bounds of the design variables are provided in Table 4.

After the design space is generated (i.e., the bounds of the design variables are determined), the optimization procedure shown in Figure 3 is followed.

The optimization procedure starts with the preliminary design (or nominal design) of the runner. Next, the input parameters from geometry (i.e., the lean and metal angles for five different span of the meridional surface) are determined. We found that the interaction between the lean angle and metal angle is negligible. Therefore, first, the metal angle is optimized separately by taking the nominal values of the lean angles, and then, optimization is performed for the lean angle by using the optimized values of the metal angles.

Optimization is performed by using ANSYS DesignXplorer tool.²² This software provides a straightforward way to set up a connection between numerical analyses and optimization. It consists of commonly used metamodel types for optimization and numerical techniques to handle with high-dimensional functions in the process. The common practice in metamodel-based optimization is to construct different types of metamodels, to evaluate their accuracies, and to use the most accurate metamodel in optimization. However, it was found that the use of the most accurate metamodel in optimization does not necessarily lead to optimum.¹⁶ Therefore, in this

Table 5. Runner design parameters.

Turbine parameters
Head: H (m)
Volumetric flow rate: Q (m ³ /s)
Specific speed: N_s
Geometric parameters
Runner dimensions:
$D_i, D_o, D_t, D_{max}, b_0, D_g, D_s, \alpha$
Blade angles:
Metal angle: ξ
Lean angle: θ

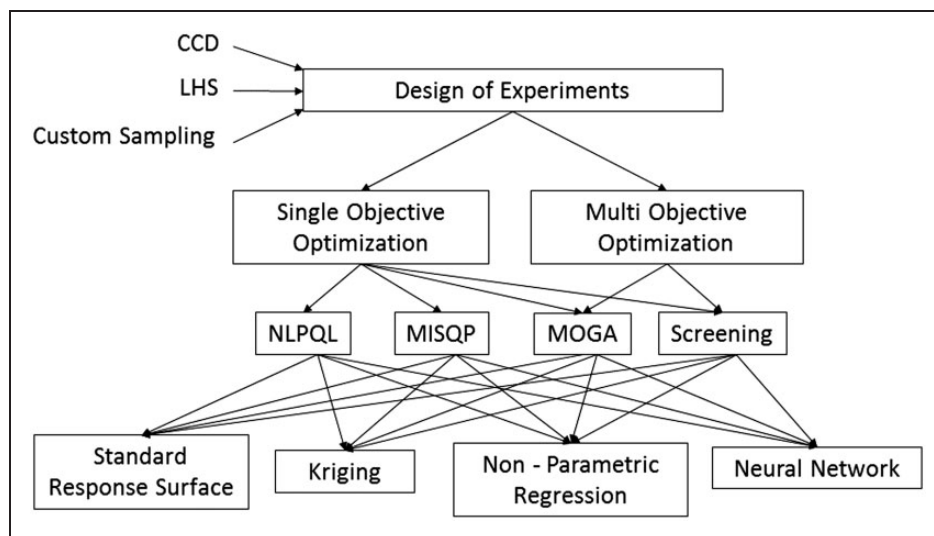


Figure 4. Procedure for generating multiple optimum candidates by using multiple optimization algorithms and metamodel types. LHS: Latin hypercube sampling; CCD: central composite design; NLPQL: nonlinear programming by quadratic Lagrangian; MISQP: mixed-integer sequential quadratic programming; MOGA: multi-objective genetic algorithm.

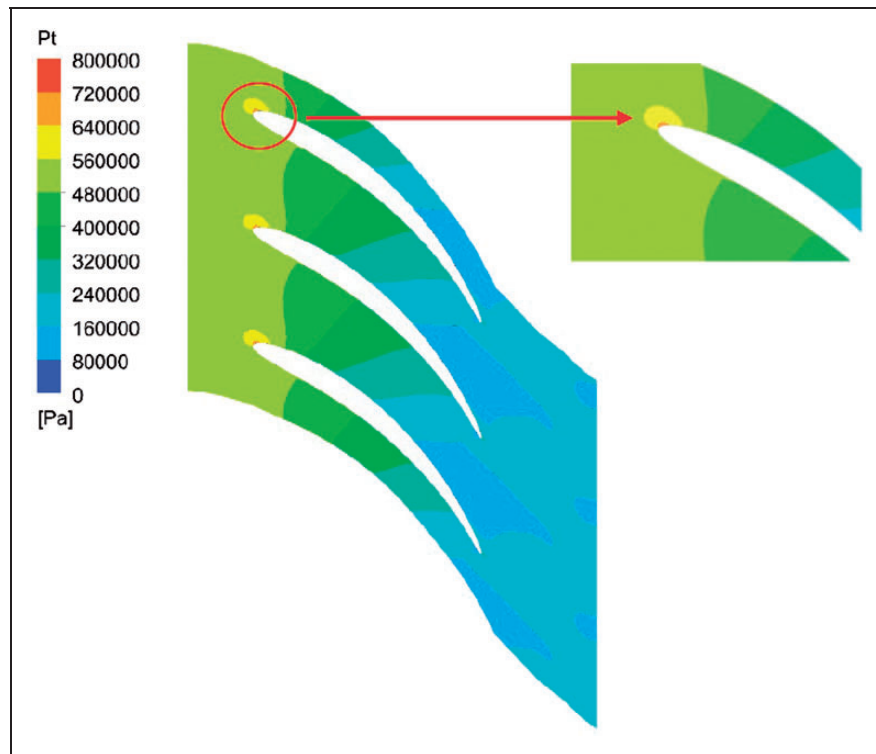


Figure 5. Total pressure distribution between runner blades.

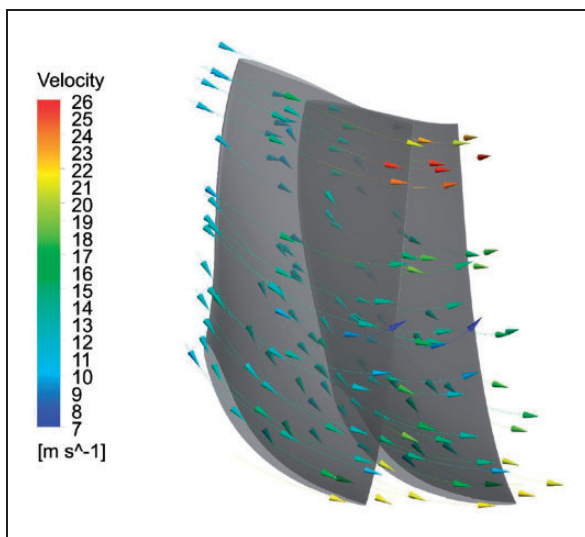


Figure 6. Velocity vectors between blades.

paper, the optimization studies are performed by using different optimizers and different metamodel types available in ANSYS DesignXplorer tool to obtain multiple optimum solution candidates, and the candidate with best performance is chosen to be the optimum configuration. Brief details of the optimization algorithms and the metamodel types used in this paper are given in Appendices 1 and 2, respectively. The procedure followed to generate multiple optimum candidates by using multiple metamodel types and optimization algorithms is shown in

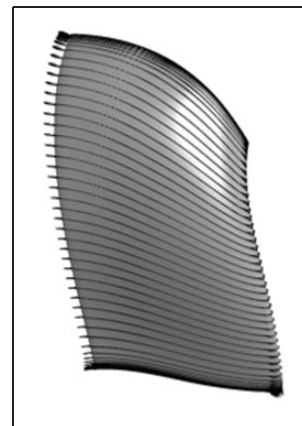


Figure 7. Velocity vectors on blades.

Figure 4. For the first optimization case (single objective optimization), four different optimizers and four different metamodel types are used, resulting in 16 optimum candidates. For the second optimization case (multi-objective optimization), on the other hand, two different optimizers and four different metamodel types are used, resulting in eight optimum candidates.

For the first optimization case, only metal angles are optimized. We found that metal angle has small effect on cavitation compared to the lean angle (see Appendix 1). For the second optimization case, on the other hand, only lean angles are optimized (see Appendix 2).

CFD analysis

In this study, CFD is used for turbine performance analyses that include characteristic flow properties and energy losses. Numerical analyses are performed by using ANSYS-CFX²³ for a single runner blade to eliminate complexity of simulations. However, to predict the whole flow characteristics in turbine runner, computational domain is reduced to the flow field between two runner blades by using periodicity condition.⁶ Periodicity condition helps to determine the

sequence of the runner blades in the analyses. Boundary conditions are defined as total pressure at the inlet and volumetric flow rate at the outlet. Since only known parameters are total pressure and volumetric flow rate, these are chosen as boundary conditions for single blade analyses. The opposite situation is valid for complete turbine runner analyses. In addition to these boundary conditions, no-slip condition is used with k-epsilon turbulence model with 10^{-5} convergence criteria. H/J/C/L topology (letters representing mesh shape around the blade) is chosen for the mesh. It is applied to one blade surface by using 250k elements. The output of CFD analyses is the efficiency, pressure, velocity, power which are found to be helpful to determine the adequacy of the turbine.²⁴

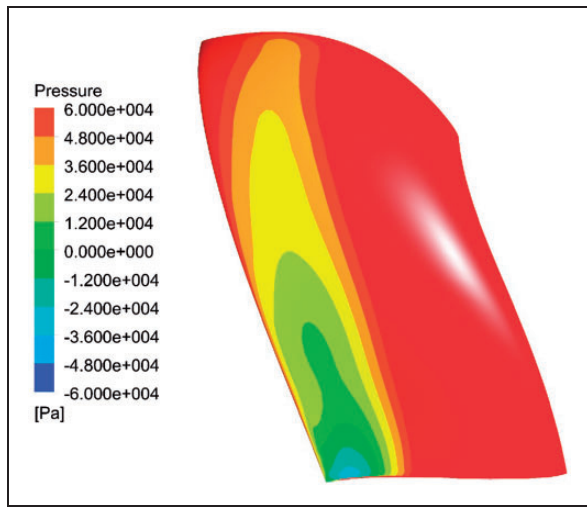


Figure 8. Pressure distribution on the blade surface.

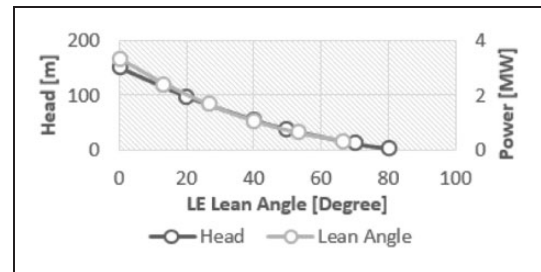


Figure 11. Effects of LE lean angle on turbine head and power. LE: leading edge.

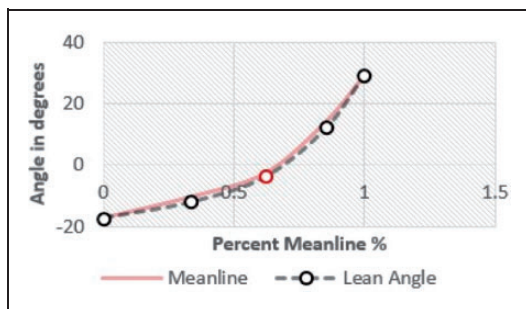


Figure 9. Specified spline point for lean angle.

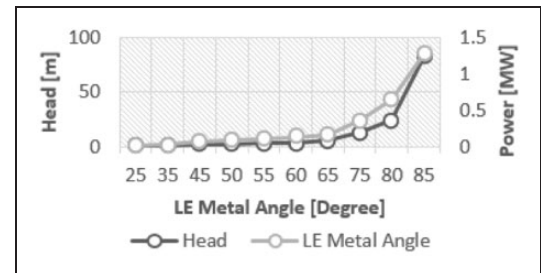


Figure 12. Effects of LE metal angle on turbine head and power. LE: leading edge.

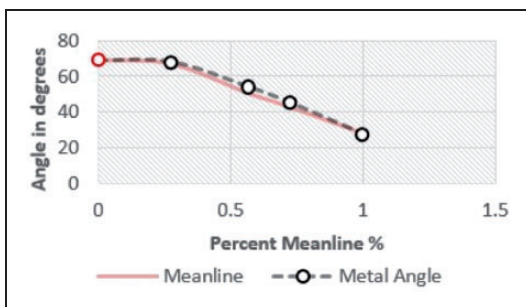


Figure 10. Specified spline point for metal angle.

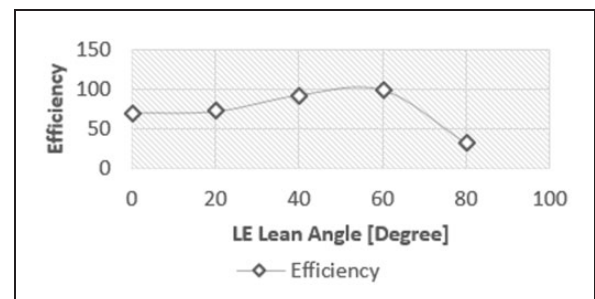


Figure 13. Effects of LE lean angle on turbine efficiency. LE: leading edge.

It is known that leak tightness is not an important concern for turbine performance; however, blade surface has an undeniable effect on efficiency and power. Therefore, smooth blade surface and leak tightness are assumed for numerical analyses. To create a smooth blade for the analyses, blade geometry is created with the help of ANSYS-BladeGen²¹ module. The general shape is generated by using turbine initial

design parameters as a first step. These are the basic turbine parameters such as head, volumetric flow rate, specific speed that provide basic dimensions of runner. As a second step, blade shape is iterated until uniform area distribution of the blade surface is obtained. To reach uniform area distribution, basic geometrical design parameters (turbine inlet and outlet diameters, guide vane height and basic blade angles) are calculated by using one-dimensional Euler equations. These parameters are summarized in Table 5. Here, ξ is the metal angle, and θ is the lean angle. D_i is the inlet diameter, D_o is the outlet diameter of the turbine, whereas D_{max} is the maximum outlet diameter. D_t is the throat diameter, which is the minimum diameter of flow passage of the runner. D_g and D_s are the guide vane and shaft diameters, respectively. b_0 is the guide vane height, and α is the guide vane angle.

For performing CFD analyses, HP Workstation Z210 Intel 64 byte operating system is used. To reduce computational time, calculations are performed with HP Intel Xeon CPU E5-26670 @

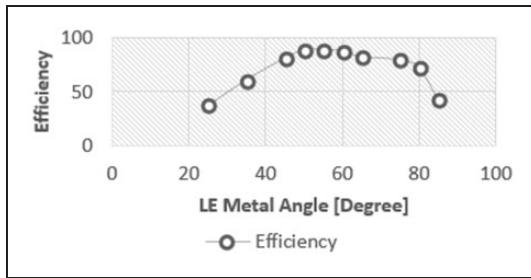


Figure 14. Effects of LE metal angle on turbine efficiency. LE: leading edge.

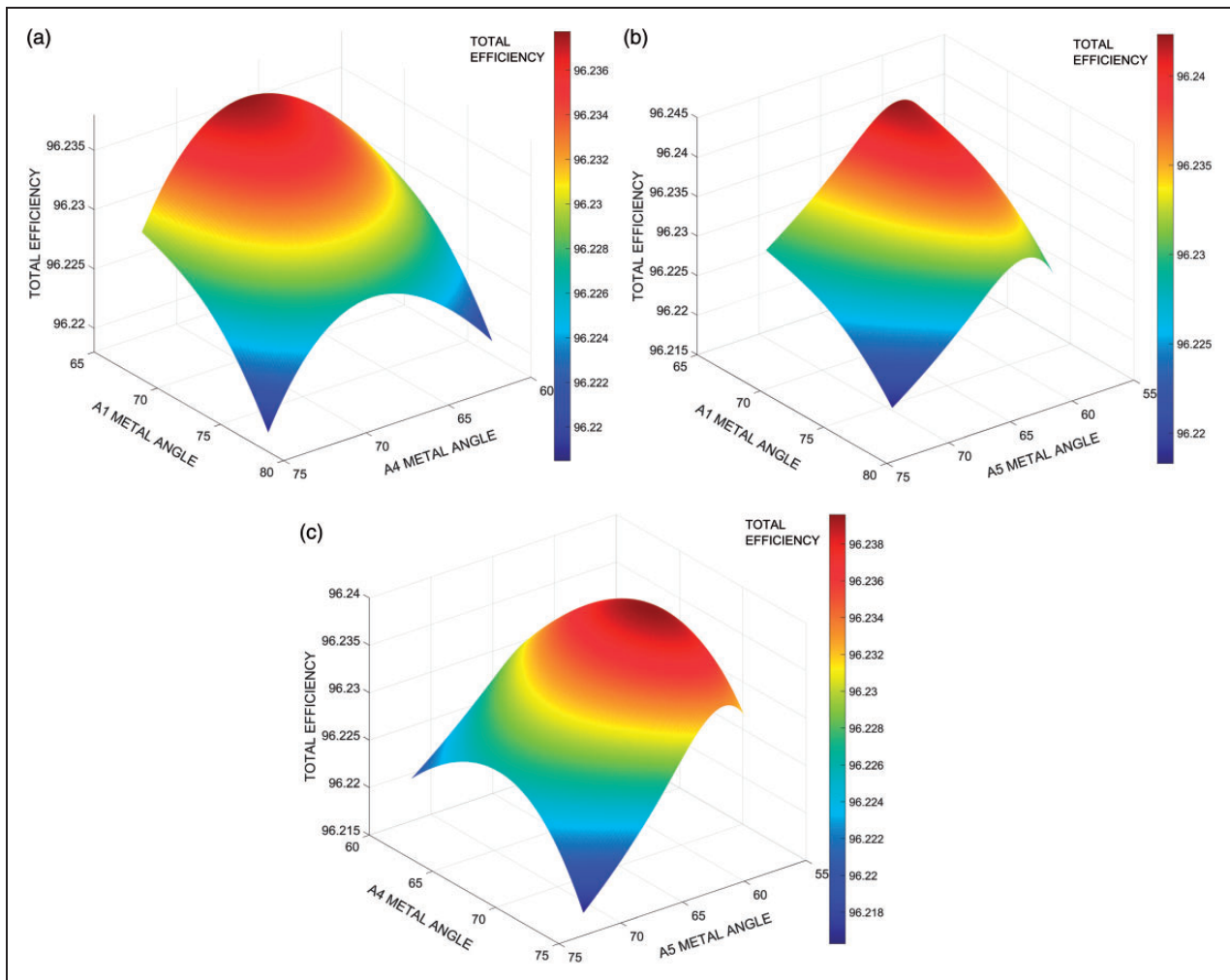


Figure 15. Response surface results for metal angle for total efficiency (a) A1 and A4 span, (b) A1 and A5 span and (c) A4 and A5 span.

2.90 GHz Cluster with 110 processors. The baseline design for the runner is taken from a previous study.²⁵ Total pressure distribution, velocity distribution and velocity vectors on the blade surface for the baseline runner design are presented in Figures 5 to 8.

Metamodel construction

Design of experiments

DoE is a systematic method which determines the location of data points in design space which are used to calculate the objective and constraint functions. Latin hypercube sampling (LHS), central composite design (CCD) and Box-Behnken design are examples of commonly used DoE. In this paper, LHS is used.

The number of training points are selected as 10 times the number of design variables. Since there exists five design variables in optimization for lean angles and optimization for metal angles, 50 training

points are used in LHS DoE. The DoE and corresponding responses are provided in Appendix 3.

Metamodel types

Metamodels are the mathematical models used to determine the relationships between the input parameters (here the design variables) and simulation outputs used in the objective and constraint functions. Metamodels simplify the optimization process by replacing computationally costly analyses models.^{26,27} In this study, five different metamodel types, namely the standard response surface, Kriging, non-parametric regression, neural network and sparse grid are used. As noted earlier, there are no specified metamodels for a given problem which guarantees finding the optimum. The selection of the appropriate metamodel type depends on the problem structure and the complexity of design. To protect against using the wrong metamodel, all metamodel types available in ANSYS DesignXplorer module are used.

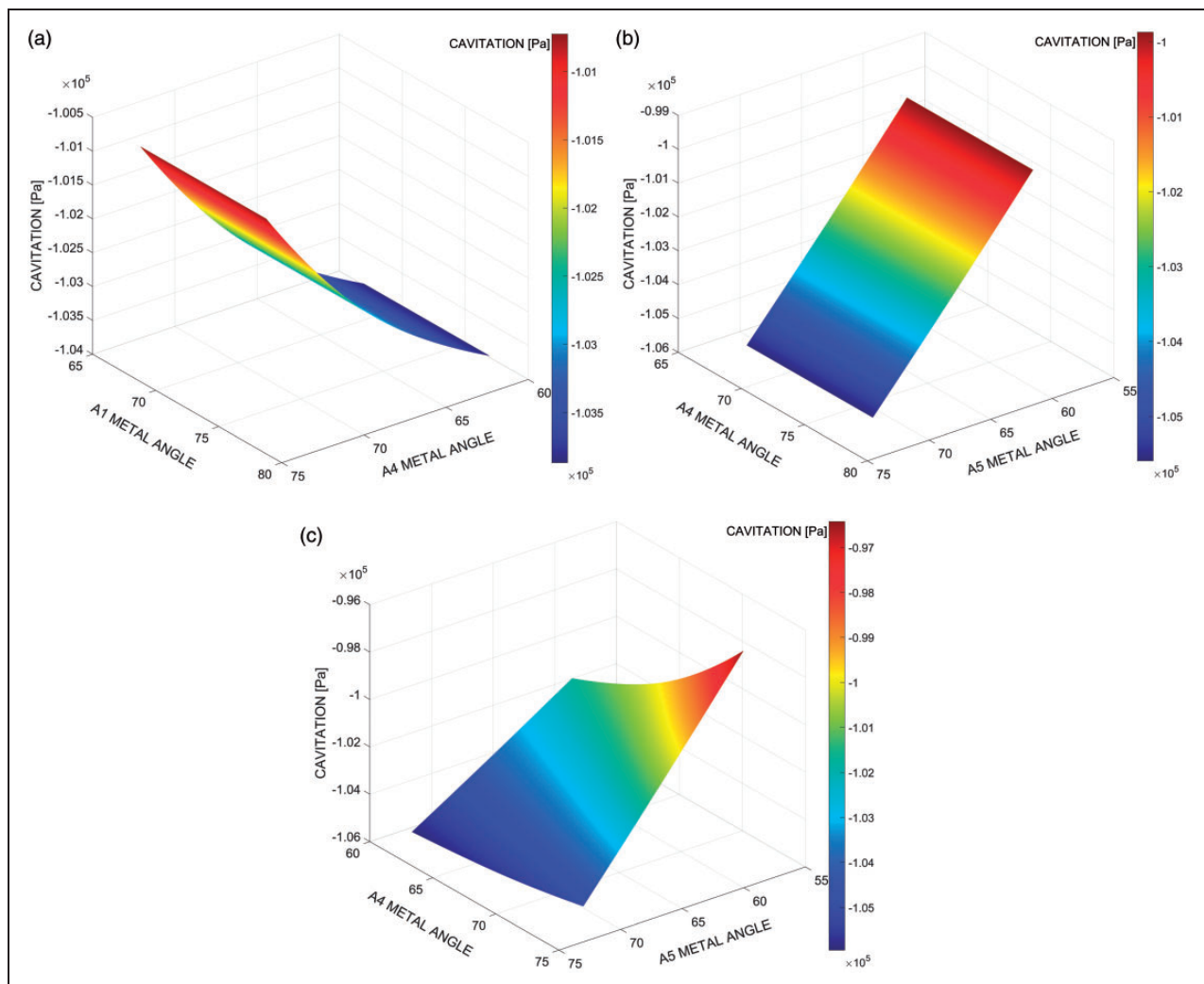


Figure 16. Response surface results for metal angle for cavitation (a) A1 and A4 span, (b) A1 and A5 span and (c) A4 and A5 span.

Results

Preliminary design evaluation

Inlet parameters are selected to find the blade curvature effects on turbine efficiency and cavitation coefficient. Therefore, inlet and outlet parameters of the optimization are chosen from the blade angles which change the blade curvature. Lean and metal angles are used to determine the optimum shape of the runner blade with curvature. Lean angle is always used for the edges of the blades. Blade metal angle of a runner blade is defined by the angle between the blade and a meridian plane, and it is measured perpendicular to the stream surface. To understand the general relation, hub and tip (shroud) points (see Figure 2) are chosen to be analyzed. These points show the variation of the mean line of blade when changes are applied.

As inlet parameters, metal and lean angles are varied as a function of meanline with fifth-order Bezier spline (B-Spline) representation. This representation of curves ensures that the line and its derivatives

are smooth to provide an ideal platform to define the shape of the blade. Five spline points are chosen as a default starting from leading edge (LE) to the trailing edge (TE). In this study, the third point of each span is defined as an input parameter for lean angle and each first point for metal angle. Figures 9 and 10 indicate the points with color red used in this study.

Preliminary design evaluation study shows that lean and metal angle have different effects on the performance of the turbine. It is found that lean angle is more important for turbine efficiency because of the curvature effect. Besides these, hub point of the metal angle and middle point of the lean angle are found to be the most effective parameters. Therefore, they are used in 3-D analyses for each span. Figures 11 to 14 show the effects of these input parameters.

Effect of the metal angles

The effect of the metal angles on the total efficiency and cavitation is shown in Figures 15 and 16, where response surface approximations are shown for

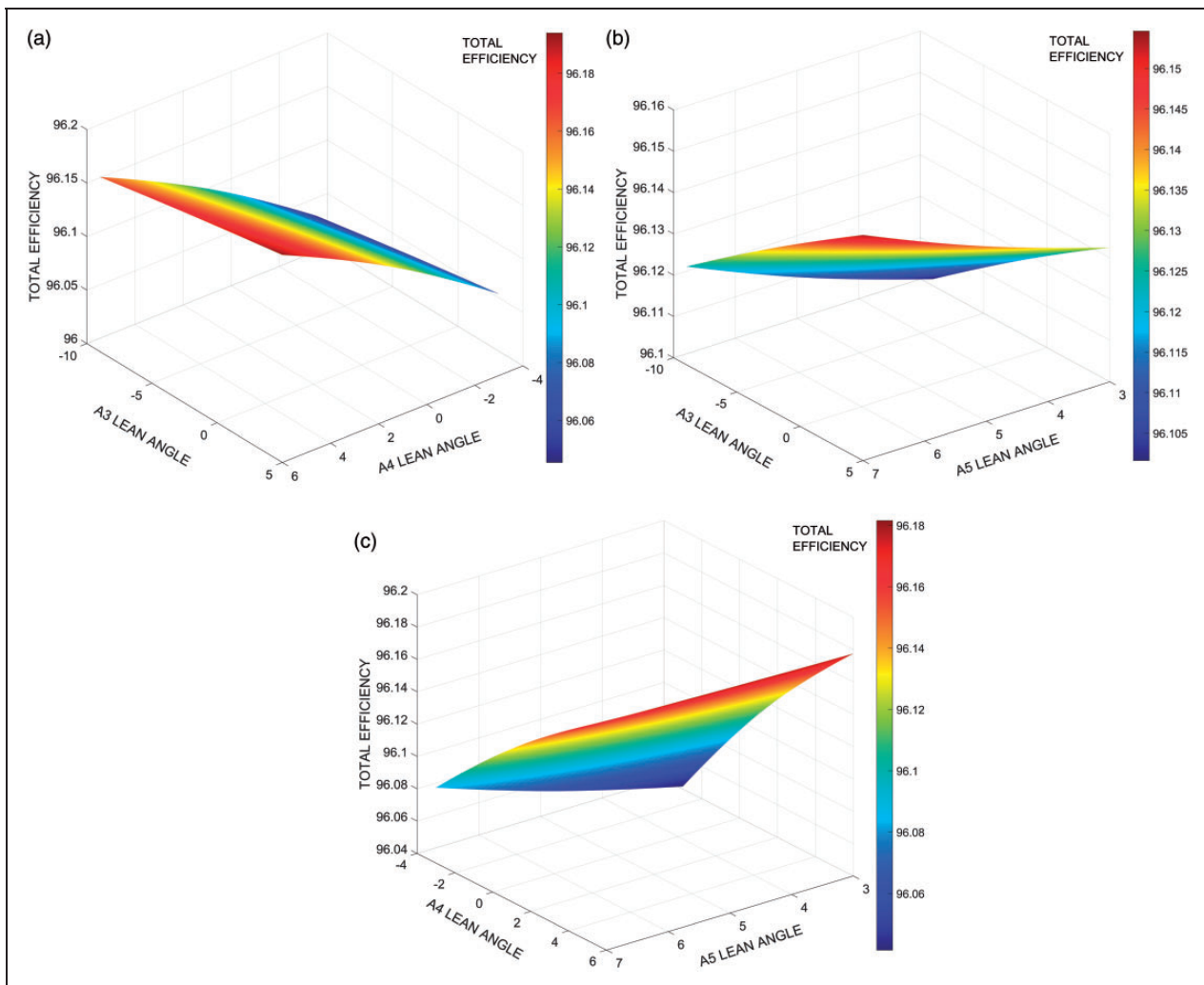


Figure 17. Response surface results for lean angle for total efficiency (a) A3 and A4 span, (b) A3 and A5 span and (c) A4 and A5 span.

depiction. Figure 15 shows that metal angle depicts different trends for each span for total efficiency. It is also observed that metal angle on A1 span reaches its peak value on A4 and A5 span. Figure 16 indicates that cavitation changes on the runner blade depending on the metal angle. On the other hand, LE and TE metal angle values are not completely related to cavitation as expected.

Effect of the lean angles

Response surface approximations shown in Figures 17 and 18 demonstrate additional features different than metal angle. By completing each other, both lean and metal angle have an important effect for efficiency of runner. The lean angle has the power to control both cavitation and efficiency. Thus, both cavitation and efficiency are defined as objective functions for the multi-objective optimization case. Figures 17 and 18 also show that A4 span in results of lean angle and metal angle affects the performance

different than others. Also, this parameter shows similar results compared to A5 span at TE.

Brief discussion of the overall results

As noted earlier, the optimization studies are carried out by using different optimizers and different meta-model types to obtain multiple optimum solution candidates for each optimization case. The optimum candidates obtained are given in Appendix 4.

For each case, after multiple optimum candidates are determined, the candidate with best performance is chosen to be the optimum configuration. The optimization results for both cases can be seen in Table 6. Contrary to expectations, the effect of metal angle on the total efficiency did not provide the expected results. Increasing metal angle means shorter blades, therefore friction decreases and efficiency was expected to get higher. As explained in the previous sections, lean and metal angle has a relation to constitute the curvature of the blade. Therefore, this can

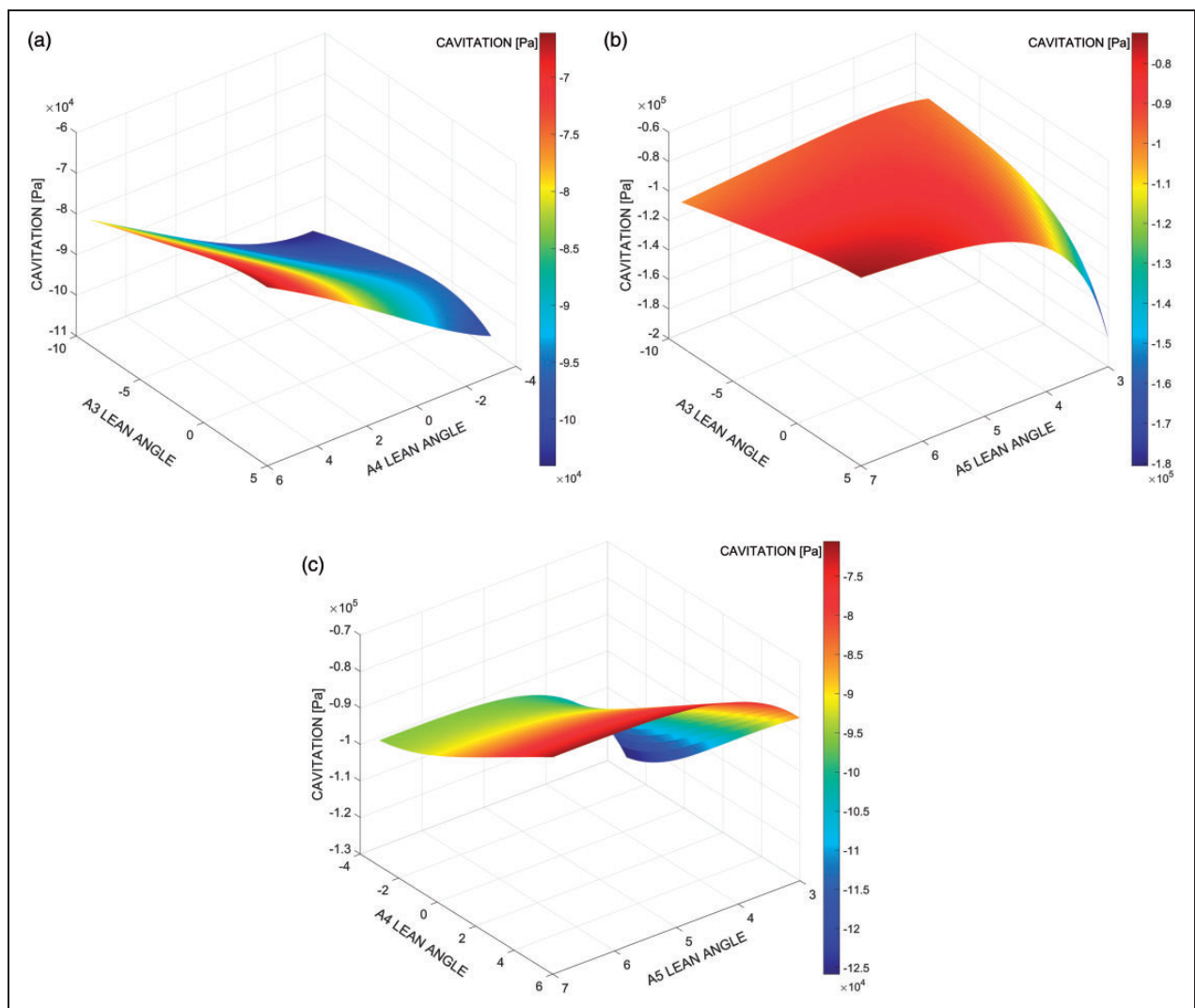


Figure 18. Response surface results for lean angle for cavitation (a) A3 and A4 span, (b) A3 and A5 span and (c) A4 and A5 span.

Table 6. Optimization results for both cases.

Design variables and responses	Reference value	Optimum value
Results for first optimization case (optimization of metal angles)		
0% Span (A1)	69.44	67.62
20% Span (A2)	68.35	66.71
50% Span (A3)	68.47	75.08
75% Span (A4)	67.38	71.13
100% Span (A5)	65.55	62.42
Cavitation (Pa)	-88,596	-99,742
Head (m)	37.26	46.88
Shaft power (MW)	0.870	1.105
Total efficiency (%)	95.60	96.13
Results for second optimization case (optimization of lean angles)		
0% Span (A1)	-18.00	-6.97
20% Span (A2)	-16.82	-6.57
50% Span (A3)	-12.61	4.33
75% Span (A4)	-6.25	5.09
100% Span (A5)	0.11	6.66
Cavitation (Pa)	-88,596	-63,789
Head (m)	37.26	44.03
Shaft power (MW)	0.870	1.038
Total efficiency (%)	95.60	96.18

be an explanation to unexpected result. On the other hand, it is obtained that lean angle is the main parameter in this study which controls both efficiency and cavitation on blades effectively. It is known that cavitation is sensitive to pressure and lean angle regulates cross flow on the runner blade to balance the pressure. When they are thought together, it can be said that results meet the expectations for lean angle.

Conclusion

A CFD driven, metamodel-based approach was presented for design and optimization of Francis type turbine runners. Preliminary design of the runner blade was used, and the optimum results for cavitation free, high-efficiency turbine were anticipated. Contrary to expectations, the effect of the metal angle on the total efficiency did not show the desired results. Increasing metal angle means shorter blades, therefore friction decreases and efficiency was expected to get higher.

The reason of the unexpected small increase in the efficiency could be that the efficiency had already been increased to a specified value in the preliminary design which was performed to obtain a uniform flow area. While the increase in the total efficiency based on a change in metal angle is 0.03%, the increase in the turbine power is 1.3% as we take the reference point as our preliminary design results. Metal angle shows a

great effect on the turbine power. Besides, if we compare the results with previous CFD studies, increment in the efficiency was calculated as 0.6%.

The effects of the lean angle were calculated by using the optimum metal angle values. All the results for the lean angle satisfied the expectations. In the case, the cavitation coefficient was reduced the cavitation bound in 50% starting from the highest value. If we compare the results with previous CFD results, we can calculate the difference as 18%.

Previously developed CFD-based methodology is integrated to the optimization process, and the results are compared to the results obtained from on-going CFD studies. Design time before optimization takes 5.5 months to complete together with pre-design process which is 15 days. After optimization, design time is reduced to 0.6 months with the pre-design process time. That is, compared to the conventional methods such as CFD, metamodel-based optimization can reduce design process time by a factor of 9.2. In addition, with the help of optimization, turbine performance is increased while reducing cavitation that occurs on the turbine runner blades which can be harmful for the turbine, reducing its life span.

Declaration of Conflicting Interests

The author(s) declared no potential conflicts of interest with respect to the research, authorship, and/or publication of this article.

Funding

The author(s) disclosed receipt of the following financial support for the research, authorship, and/or publication of this article: This study is financially supported by the Ministry of Development of Turkey. The computations are performed at TOBB ETU Center for Hydro Energy Research (ETU Hydro), CFD Laboratory.

References

1. Paish O. Small hydro power: technology and current status. *Renew Sustain Energ Rev* 2002; 6: 537–556.
2. Daneshkakh K and Zangeneh M. Parametric design of a Francis turbine runner by means of a three-dimensional inverse design method. *IOP Conf Ser Earth Environ Sci* 2010; 12: 012058.
3. Sallaberger MJ. Quasi-three-dimensional and three-dimensional flow calculation in a Francis turbine. In: *ASME international gas turbine and aeroengine congress and exhibition, Birmingham*, 10–13 June 1996, pp.V001T01A006. New York: American Society of Mechanical Engineers.
4. Krivchenko GI, Kochin V and Semenov S. *Hydraulic machines: turbines and pumps*. Boca Raton, FL: Lewis publishers, 1994.
5. Drtina P and Sallaberger M. Hydraulic turbines basic principles and state-of-the-art computational fluid dynamics applications. *Proc IMechE, Part C: J Mechanical Engineering Science* 1999; 213: 85–102.
6. Lopez LF. *Surface parameterization and optimum design methodology for hydraulic turbines*. PhD Thesis, École Polytechnique Fédérale de Lausanne, Lausanne, 2006.

7. Albuquerque RF, Manzanares-Filho N and Oliveira W. Conceptual optimization of axial-flow hydraulic turbines with non-free vortex design. *Proc IMechE, Part A: J Power and Energy* 2007; 221: 713–725.
8. Wu J, Shimmei K, Tani K, et al. CFD-based design optimization for hydro turbines. *J Fluid Eng* 2007; 129: 159–168.
9. Nilsson H and Davidson L. Validations of CFD against detailed velocity and pressure measurements in water turbine runner flow. *Int J Numer Meth Fluid* 2003; 41: 863–879.
10. Derakhshan S and Mostafavi A. Optimization of GAMM Francis turbine runner. *World Acad Sci Eng Technol* 2011; 59: 717–723.
11. Thum S and Schilling R. Optimization of hydraulic machinery bladings by multilevel CFD techniques. *Int J Rotat Mach* 2005; 2005: 161–167.
12. Georgopoulou H, Kyriacou S, Giannakoglou K, et al. Constrained multi-objective design optimization of hydraulic components using a hierarchical metamodel assisted evolutionary algorithm. Part 1: Theory. In: *24th IAHR symposium on hydraulic machinery and systems, Brazil, 27–31 October 2008*.
13. Nakamura K and Kurosawa S. Design optimization of a high specific speed Francis turbine using multi-objective genetic algorithm. *Int J Fluid Mach Syst* 2009; 2: 102–109.
14. Enomoto Y, Kurosawa S and Kawajiri H. Design optimization of a high specific speed Francis turbine runner. *IOP Conf Ser Earth Envir Sci* 2006; 15: 032010.
15. Kawajiri H, Enomoto Y and Kurosawa S. Design optimization method for Francis turbine. *IOP Conf Ser Earth Environ Sci* 2014; 22: 012026.
16. Acar E, Guler M, Gerceker B, et al. Multi-objective crashworthiness optimization of tapered thin-walled tubes with axisymmetric indentations. *Thin Wall Struct* 2011; 49: 94–105.
17. Marler RT and Arora JS. Survey of multi-objective optimization methods for engineering. *Struct Multidiscipl Optim* 2004; 26: 369–395.
18. Kutz M. *Mechanical engineers' handbook, design, instrumentation, and controls*. Mechanical engineers' handbook. Bognor Regis: Wiley, 2015. ISBN: 9781118930830.
19. Brekke H. A discussion on turbine design for safe operation. *IOP Conf Ser Earth Environ Sci* 2012; 15: 022003.
20. Marier S and Theroux E. *Compact blade for runner of Francis turbine and method for configuring runner*. US Patent App.14/353,670, 2014.
21. ANSYS Bladegen, version 15.0, User Manual, 2015.
22. ANSYS DesignXplorer. Academic Research Release 2015, p.15.
23. ANSYS CFX, version 15.0, User Manual, 2015.
24. Lipej A. Optimization method for the design of axial hydraulic turbines. *Proc IMechE, Part A: J Power and Energy* 2004; 218: 43–50.
25. Ayancik F, Celebioglu K and Aradag S. Parametrical and theoretical design of a Francis turbine runner with the help of computational fluid dynamics. In: *International conference on heat transfer, fluid mechanics and thermodynamics*, Orlando, Florida, 14–16 July 2014.
26. Barton RR and Meckesheimer M. Metamodel-based simulation optimization. *Handbook Oper Res Manag Sci* 2006; 13: 535–574.
27. Park GJ. *Analytic methods for design practice*. London, UK: Springer Science & Business Media, 2007.
28. Deb K, Pratap A, Agarwal S, et al. A fast and elitist multiobjective genetic algorithm: NSGA-II. *IEEE Trans Evol Comput* 2002; 6: 182–197.
29. Myers RH and Montgomery DC. *Response surface methodology: process and product optimization using designed experiments*. New York, NY: Wiley, 2002.
30. Sacks J, Welch WJ, Mitchell TJ, et al. Design and analysis of computer experiments. *Stat Sci* 1989; 4: 409–435.
31. Simpson TW, Mauery TM, Korte JJ, et al. Kriging models for global approximation in simulation based multidisciplinary design optimization. *AIAA J* 2001; 39: 2233–2241.
32. Vapnik V. *The nature of statistical learning theory*. New York, NY: Springer, 1995.
33. Gunn SR. *Support vector machines for classification and regression*. Technical Report, University of Southampton, UK, 1997.

Appendix I: The optimization methods used

In this paper, different optimizers of ANSYS DesignXplorer tool are used for optimization: NLPQL (nonlinear programming by quadratic Lagrangian), MISQP (mixed-integer sequential quadratic programming), MOGA and screening. NLPQL and MISQP are gradient-based optimization methods, whereas MOGA and screening are population based.

Nonlinear programming by quadratic Lagrangian

The basic idea in NLPQL is to construct a sequence of quadratic programming sub-problems obtained through quadratic approximation of the Lagrangian function and linear approximation of the constraint functions.²² In NLPQL, Hessian updating is performed through a quasi-Newton formula, and the stabilization is achieved through an additional line search. NLPQL works well for medium size and well-scaled problems.

Mixed-integer sequential quadratic programming

MISQP uses a modified sequential quadratic programming approach, where quadratic approximation of the Lagrangian function and linear approximation of the constraint functions are sequentially generated, and a mixed-integer approach is used to solve the optimization problem by using branch-and-cut method.²² The stabilization of MISQP is achieved through a trust region method.

Multi-objective genetic algorithm

MOGA is a hybrid variant of the non-dominated sorted genetic algorithm-II.²⁸ MOGA supports multiple objective functions and aims at finding the global

minimum. The default setting for the number of initial samples is 10 times the number of input parameters,²² and this setting is used in this paper.

Screening

Screening is based on the Shifted Hammersley sampling strategy, where the design space is populated uniformly by an unbiased low-discrepancy quasi-random number sequence.²²

Appendix 2: The metamodel types used

In this paper, four different metamodel types are used: Standard response surface, Kriging, non-parametric regression and neural network.

Standard response surface

The standard response surface is based on the use of full second-order polynomial to define the relationship between the input and output parameters, and it can be expressed as²⁹

$$\hat{f}(\mathbf{x}) = b_0 + \sum_{i=1}^L b_i x_i + \sum_{i=1}^L b_{ii} x_i^2 + \sum_{i=1}^{L-1} \sum_{j=i+1}^L b_{ij} x_i x_j \quad (4)$$

where \hat{f} is the response surface approximation of the actual response function, f , L is the number of variables in the input vector \mathbf{x} and b_0 , b_i , b_{ii} , b_{ij} are the unknown coefficients to be determined by the least squares technique.

Kriging

Kriging model estimates the response in the following form³⁰

$$\hat{f}(x) = p(x) + Z(x) \quad (5)$$

where \hat{f} is the predicted response, p is a known polynomial that globally approximates the response and Z is the stochastic component that generates deviations such that the Kriging model interpolates the sampled response data. The stochastic component has a mean value of zero and covariance of

$$COV[Z(x_i), Z(x_j)] = \sigma^2 \mathbf{R}[R(x_i, x_j)] \quad (6)$$

where \mathbf{R} is $N \times N$ correlation matrix, N is the number of training points, $R(x_i, x_j)$ is correlation function between the two training points x_i and x_j . Mostly, the correlation function is chosen as Gaussian, that is

$$R(\theta) = \prod_{k=1}^L \exp(-\theta_k d_k^2) \quad (7)$$

where L is the number of variables, $d_k = x_k^i - x_k^j$ is the distance between the k th components of the two training points x_i and x_j and θ_k is the unknown parameters to be determined.

Once the correlation function has been selected, the response f is predicted as

$$\hat{f}(\mathbf{x}) = \hat{\beta} + \mathbf{r}^T(\mathbf{x})\mathbf{R}^{-1}(\mathbf{f} - \hat{\beta}\mathbf{p}) \quad (8)$$

where $\mathbf{r}^T(\mathbf{x})$ is the correlation vector of length N between a prediction point \mathbf{x} and the N sampling points, \mathbf{f} represents the responses at the N points and \mathbf{p} is an L -vector of ones (if $p(x)$ is taken constant). The vector \mathbf{r} and scalar $\hat{\beta}$ are given by

$$\mathbf{r}^T(x) = [R(x, x^1), R(x, x^2), \dots, R(x, x^N)]^T \quad (9)$$

$$\hat{\beta} = (\mathbf{p}^T \mathbf{R}^{-1} \mathbf{p})^{-1} \mathbf{p}^T \mathbf{R}^{-1} \mathbf{f} \quad (10)$$

The variance of the output model is estimated as

$$\hat{\sigma}^2 = \frac{(\mathbf{f} - \hat{\beta}\mathbf{p})^T \mathbf{R}^{-1} (\mathbf{f} - \hat{\beta}\mathbf{p})}{N} \quad (11)$$

The unknown parameters θ_k can be estimated by solving the following problem³¹

$$\begin{aligned} \text{Max } \Phi(\Theta) &= \frac{-[N \ln(\hat{\sigma}^2) + \ln|\mathbf{R}|]}{2} \\ \text{s.t. } \Theta &> 0 \end{aligned} \quad (12)$$

where Θ is the vector of unknown parameters θ_k and both $\hat{\sigma}$ and \mathbf{R} are functions of Θ .

Non-parametric regression

Non-parametric regression is mainly used to predict high-nonlinear responses, and it is basically a support vector machine (SVM).³² SVMs are originally developed for classification and then extended to regression.

When used for classification, the basic idea is to create a hyperplane which separates the data into classes such that the margin is maximized. If the data classes have values of -1 and $+1$, the separating hyperplane can be defined through

$$\langle \mathbf{w}, \mathbf{x} \rangle + b = 0 \quad (13)$$

where \mathbf{w} is the vector of hyperplane coefficients, \mathbf{x} is the vector of data points, b is the bias and $\langle \mathbf{w}, \mathbf{x} \rangle$ indicates the scalar product of \mathbf{w} and \mathbf{x} . Similarly, the support hyperplanes can be defined through

$$\langle \mathbf{w}, \mathbf{x} \rangle + b = -1 \text{ and } \langle \mathbf{w}, \mathbf{x} \rangle + b = +1 \quad (14)$$

The margin between two support hyperplanes is $2/\|\mathbf{w}\|$. Therefore, the hyperplanes can be formed by solving the following optimization problem

$$\begin{aligned} \min \quad & \frac{1}{2} \|\mathbf{w}\|^2 \\ \text{s.t.} \quad & y_i(\langle \mathbf{w}, \mathbf{x} \rangle + b) \geq 1 \end{aligned} \quad (15)$$

where the constraint reflects the fact that no sample can lie between the support hyperplanes. If the classes are linearly separable, a hyperplane separating the data into classes can be found in the original variable space. For the case of nonlinearly separable classes, on the other hand, the original variable space is projected to a feature space using a nonlinear Kernel function. In the feature space, the classification problem is similar to that of the linearly separable case. Widely used kernel functions include polynomials, Gaussian functions, Fourier series and splines.^{32,33}

When used for regression, the hyperplane is used to categorize a subset of the input sample vectors (called support vectors) that are assumed to be sufficient to represent the response.

Neural network

The neural network metamodel is composed of neurons, which are connected to each other using weights that carry the information. The functionality of neural networks is based on biological neurons. A set of training patterns are used for learning. A neural network consists of an input layer, hidden layers and an output layer as shown in Figure 19. Figure 19 shows the basics of a feed forward architecture that is common mostly in engineering applications. It consists of two hidden layers; however, a network may consist of any number of hidden layers in order to accurately predict the response of interest.

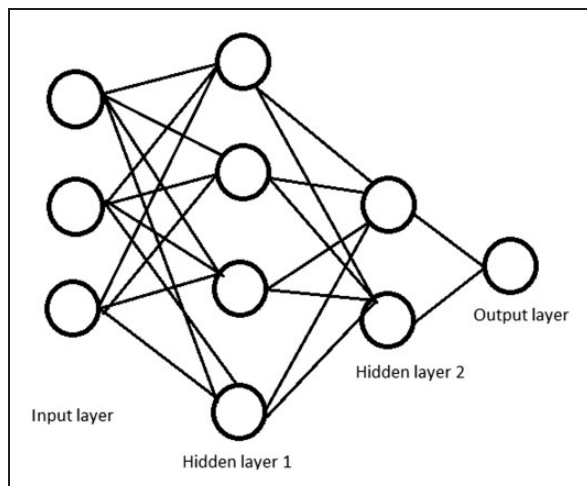


Figure 19. A feed forward neural network architecture.

Appendix 3: DoE and corresponding responses

DoE and the corresponding responses for metamodels constructed to relate the metal angles to the responses are given in Table 7. It is seen that the maximum efficiency obtained at the data points is 96.128%, while the minimum cavitation (the absolute value) obtained at the data points is -94.3 kPa, which is larger than the desired value of -66 kPa. Therefore, it is not possible to satisfy the cavitation constraint by adjusting the metal angles in the first optimization case, and the cavitation is used as another objective function in the second optimization case, and the desired cavitation pressure level is obtained by changing the lean angles.

DoE and the corresponding responses for metamodels constructed to relate the lean angles to the responses are given in Table 8. It is seen that the maximum efficiency obtained at the data point is 96.184%, while the minimum cavitation (the absolute value) obtained at the data point is -62.5 kPa, smaller than the desired value of -66 kPa. Therefore, it would be possible to obtain the desired cavitation pressure level is obtained by changing the lean angles.

Appendix 4: Optimum candidates for each optimization case

Sixteen optimum candidates for the first optimization case are listed in Table 9. The optimum candidate #13 yields the maximum efficiency value, so that candidate is taken to be the optimum design. Cavitation values are not provided in the table since the optimization of metal angles only is not sufficient enough to obtain the desired cavitation pressure level.

Eight optimum candidates for the first optimization case are listed in Table 10. Since this case is a multi-objective optimization case, we need to evaluate both objectives of the optimum candidates. Table 10 shows that no candidate can dominate other candidates in terms of both objectives. For instance, optimum candidate #7 yields the minimum cavitation (but not the maximum efficiency), whereas optimum candidate #1 yields the maximum efficiency (but not the minimum cavitation). To determine the optimum configuration, we define an aggregate objective function (AOF, see equation (16)) in terms of both objectives, and the optimum candidate having the minimum AOF value is declared as the optimum configuration. Table 10 shows that the optimum candidate #1 yields the minimum AOF value, so it is taken to be the optimum design

$$\text{AOF} = -\frac{f_1}{f_{10}} + \frac{f_2}{f_{20}} \quad (16)$$

Table 7. Design of experiments and corresponding responses (for first optimization case).

#	A1 (°)	A2 (°)	A3 (°)	A4 (°)	A5 (°)	Cavitation (Pa)	Head (m)	Shaft power (W)	Total efficiency (%)
1	71.30	66.70	75.20	61.45	62.80	-106,100	47.105	1,110,130	96.112
2	73.10	72.50	69.60	62.81	59.66	-101,417	46.825	1,103,600	96.119
3	67.90	74.50	66.40	67.71	64.12	-100,722	46.602	1,098,400	96.122
4	72.10	71.90	75.00	73.15	62.02	-101,198	46.751	1,101,970	96.127
5	68.30	68.30	67.20	70.16	68.84	-106,347	46.572	1,097,580	96.112
6	76.90	69.10	71.60	61.18	70.41	-106,218	46.889	1,104,970	96.105
7	71.90	73.30	74.60	65.80	67.79	-106,385	46.931	1,106,130	96.120
8	76.70	72.10	65.60	66.89	61.23	-100,499	46.874	1,104,800	96.122
9	69.50	69.70	68.60	69.61	64.38	-100,158	46.636	1,099,230	96.125
10	68.90	75.90	66.60	68.25	69.10	-101,358	46.593	1,098,180	96.122
11	70.30	66.10	67.00	64.72	63.59	-102,916	46.900	1,105,400	96.121
12	68.70	70.90	70.00	62.00	70.15	-104,921	46.807	1,103,120	96.113
13	71.10	70.50	68.20	64.44	69.63	-103,484	46.718	1,101,050	96.115
14	73.70	75.30	69.20	69.07	65.69	-101,957	46.679	1,100,220	96.123
15	70.10	67.90	75.40	72.06	59.92	-96,676	46.793	1,102,940	96.127
16	75.50	73.90	73.80	64.17	61.49	-104,672	47.012	1,108,020	96.118
17	75.10	71.10	67.40	61.72	66.48	-103,279	46.825	1,103,520	96.110
18	72.90	75.50	73.40	70.43	71.20	-104,156	46.718	1,101,080	96.117
19	68.50	70.10	71.20	63.36	60.97	-100,555	46.976	1,107,280	96.128
20	68.10	75.70	72.00	70.70	60.71	-103,638	46.701	1,100,720	96.122
21	70.90	72.30	70.40	71.79	63.33	-103,735	46.669	1,099,920	96.118
22	75.70	67.70	73.60	73.42	65.43	-97,812	46.728	1,101,330	96.120
23	77.10	74.70	72.60	69.34	59.39	-103,842	46.847	1,104,050	96.112
24	69.10	67.30	69.40	63.90	60.18	-99,569	46.789	1,102,820	96.123
25	74.30	71.30	66.80	73.96	66.22	-100,812	46.521	1,096,290	96.105
26	72.70	69.90	71.00	66.35	68.05	-106,204	46.759	1,102,030	96.117
27	74.90	69.50	72.80	64.99	67.53	-105,751	46.866	1,104,500	96.112
28	73.50	67.50	68.40	69.88	71.99	-107,717	46.651	1,099,350	96.104
29	77.30	69.30	66.20	71.52	65.17	-98,899	46.674	1,100,020	96.116
30	70.50	73.70	70.80	63.63	63.85	-105,833	47.017	1,108,200	96.124
31	74.50	74.30	68.00	71.24	71.46	-105,193	46.550	1,096,970	96.105
32	75.30	73.50	66.00	60.64	63.07	-102,157	46.964	1,106,830	96.113
33	71.50	70.30	71.80	65.26	67.00	-106,519	46.886	1,105,110	96.124
34	75.90	73.10	73.20	60.91	68.58	-106,706	46.992	1,107,410	96.107
35	70.70	74.10	71.40	72.60	67.27	-101,042	46.659	1,099,750	96.123
36	69.70	66.90	67.60	67.44	68.32	-104,087	46.690	1,100,450	96.120
37	76.50	71.50	70.60	63.08	69.89	-103,805	46.873	1,104,690	96.114
38	76.30	68.50	73.00	70.97	70.68	-110,902	46.740	1,101,400	96.100
39	72.50	66.30	70.20	72.33	61.76	-94,320	46.731	1,101,470	96.125
40	77.50	75.10	72.20	67.98	59.13	-109,573	46.951	1,106,370	96.099
41	72.30	68.70	69.00	66.08	62.54	-102,670	46.876	1,104,890	96.126
42	71.70	74.90	68.80	62.27	69.36	-102,104	46.828	1,103,660	96.118
43	73.90	67.10	67.80	67.16	60.44	-98,840	46.823	1,103,590	96.121
44	69.30	68.90	74.00	65.53	65.95	-106,297	46.936	1,106,270	96.123
45	74.70	68.10	74.80	68.52	71.73	-106,448	46.856	1,104,230	96.109
46	74.10	72.70	74.40	72.88	70.94	-103,844	46.701	1,100,640	96.115
47	76.10	66.50	69.80	66.62	62.28	-104,166	46.908	1,105,560	96.119
48	73.30	70.70	65.80	73.69	64.64	-99,720	46.500	1,095,830	96.107
49	69.90	72.90	74.20	62.54	64.90	-103,138	47.004	1,107,850	96.120
50	67.70	71.70	72.40	68.80	66.74	-103,550	46.787	1,102,760	96.123
Min	67.70	66.10	65.60	60.64	59.13	-110,902	46.500	1,095,830	96.099
Max	77.50	75.90	75.40	73.96	71.99	-94,320	47.105	1,110,130	96.128

Table 8. Design of experiments and corresponding responses (for second optimization case).

#	A1 (°)	A2 (°)	A3 (°)	A4 (°)	A5 (°)	Cavitation (Pa)	Head (m)	Shaft power (W)	Total efficiency (%)
1	-6.08	-10.95	4.58	-2.37	4.16	-126,184	46.252	1,089,300	96.064
2	-3.20	-2.25	-3.26	-1.47	3.20	-120,071	46.504	1,095,330	96.071
3	-11.52	0.75	-7.74	1.77	4.56	-104,967	46.156	1,087,010	96.061
4	-4.80	-3.15	4.30	5.37	3.92	-83,207	44.345	1,045,620	96.175
5	-10.88	-8.55	-6.62	3.39	6.00	-94,849	45.565	1,073,690	96.114
6	2.88	-7.35	-0.46	-2.55	6.48	-92,858	46.155	1,087,380	96.094
7	-5.12	-1.05	3.74	0.51	5.68	-84,390	45.085	1,062,530	96.128
8	2.56	-2.85	-8.86	1.23	3.68	-94,022	46.230	1,089,160	96.096
9	-8.96	-6.45	-4.66	3.03	4.64	-87,217	45.522	1,072,890	96.134
10	-9.92	2.85	-7.46	2.13	6.08	-93,656	45.540	1,073,100	96.113
11	-7.68	-11.85	-6.90	-0.21	4.40	-106,361	46.770	1,101,540	96.068
12	-10.24	-4.65	-2.70	-2.01	6.40	-101,524	46.186	1,087,800	96.068
13	-6.40	-5.25	-5.22	-0.39	6.24	-103,016	46.107	1,086,160	96.088
14	-2.24	1.95	-3.82	2.67	5.04	-82,058	45.102	1,063,090	96.141
15	-8.00	-9.15	4.86	4.65	3.28	-111,957	44.790	1,055,920	96.158
16	0.64	-0.15	2.62	-0.57	3.76	-114,567	45.598	1,074,350	96.103
17	0.00	-4.35	-6.34	-2.19	5.28	-95,379	46.494	1,095,200	96.081
18	-3.52	2.25	2.06	3.57	6.72	-69,954	44.170	1,041,560	96.183
19	-10.56	-5.85	-1.02	-1.11	3.60	-117,156	46.344	1,091,540	96.070
20	-11.20	2.55	0.10	3.75	3.52	-96,479	44.960	1,059,730	96.141
21	-6.72	-2.55	-2.14	4.47	4.32	-76,103	44.913	1,058,840	96.160
22	0.96	-9.45	2.34	5.55	4.96	-70,531	44.388	1,046,540	96.168
23	3.20	1.05	0.94	2.85	3.12	-106,099	45.056	1,062,090	96.150
24	-9.60	-10.05	-3.54	-0.75	3.36	-112,620	46.760	1,101,310	96.067
25	-1.28	-4.05	-7.18	5.91	5.20	-76,871	44.710	1,054,180	96.173
26	-3.84	-6.15	-1.30	0.87	5.76	-92,524	45.449	1,070,980	96.117
27	-0.32	-6.75	1.22	-0.03	5.60	-89,046	45.487	1,071,850	96.113
28	-2.56	-9.75	-4.94	3.21	6.96	-89,866	45.233	1,066,050	96.130
29	3.52	-7.05	-8.02	4.29	4.88	-85,498	45.422	1,070,840	96.160
30	-7.36	-0.45	-1.58	-0.93	4.48	-91,342	45.945	1,082,320	96.085
31	-0.96	0.45	-5.50	4.11	6.80	-80,863	44.648	1,052,400	96.144
32	0.32	-0.75	-8.30	-2.91	4.24	-104,433	46.970	1,105,870	96.034
33	-5.76	-5.55	-0.18	0.15	5.44	-91,726	45.644	1,075,480	96.108
34	1.28	-1.35	1.78	-2.73	5.92	-91,482	45.897	1,081,120	96.079
35	-7.04	0.15	-0.74	5.01	5.52	-73,400	44.388	1,046,490	96.164
36	-8.64	-10.65	-6.06	1.59	5.84	-102,015	46.065	1,085,320	96.101
37	2.24	-3.75	-1.86	-1.29	6.32	-89,477	45.764	1,078,440	96.119
38	1.92	-8.25	1.50	3.93	6.56	-69,723	44.320	1,045,010	96.175
39	-4.16	-11.55	-2.42	4.83	3.84	-85,558	45.217	1,065,860	96.147
40	3.84	1.65	0.38	1.95	3.04	-112,120	45.223	1,065,860	96.134
41	-4.48	-7.95	-4.10	0.69	4.08	-94,636	46.124	1,086,690	96.099
42	-5.44	1.35	-4.38	-1.83	6.16	-99,579	45.965	1,082,630	96.070
43	-1.92	-10.35	-5.78	1.41	3.44	-96,850	46.302	1,090,860	96.096
44	-9.28	-7.65	2.90	0.33	5.12	-86,627	45.508	1,072,340	96.114
45	-0.64	-8.85	4.02	2.31	6.88	-72,043	44.550	1,050,440	96.176
46	-1.60	-1.95	3.46	5.19	6.64	-62,475	43.697	1,030,420	96.184
47	1.60	-11.25	-2.98	1.05	4.00	-95,155	46.017	1,084,210	96.101
48	-2.88	-4.95	-8.58	5.73	4.72	-82,280	45.154	1,064,570	96.164
49	-8.32	-1.65	3.18	-1.65	4.80	-91,814	45.794	1,078,810	96.090
50	-11.84	-3.45	0.66	2.49	5.36	-91,072	45.435	1,070,050	96.063
MIN	-11.84	-11.85	-8.86	-2.91	3.04	-126,184	43.697	1,030,420	96.034
MAX	3.84	2.85	4.86	5.91	6.96	-62,475	46.970	1,105,870	96.184

Table 9. Multiple optimum candidates for the first optimization case (maximum efficiency is shown in bold fonts).

#	Metamodel	Optimizer	A1	A2	A3	A4	A5	Head (m)	Shaft power (MW)	η (%)
1	KR	MOGA	68.45	71.25	75.38	70.88	64.34	46.84	1,104,000	96.130
2	KR	Screening	67.60	72.60	75.50	69.83	62.54	46.89	1,105,257	96.131
3	KR	NLPQL	72.60	71.00	70.50	67.30	65.56	46.79	1,102,770	96.123
4	KR	MISQP	72.60	71.00	70.50	67.30	65.56	46.79	1,102,770	96.123
5	NPR	MOGA	69.75	70.03	70.73	66.07	62.91	46.93	1,106,118	96.131
6	NPR	Screening	74.20	73.87	72.65	72.04	61.92	46.70	1,100,870	96.129
7	NPR	NLPQL	72.60	71.00	70.50	67.30	65.56	46.79	1,102,795	96.123
8	NPR	MISQP	72.60	71.00	70.50	67.30	65.56	46.79	1,102,795	96.123
9	NN	MOGA	67.74	69.97	74.32	66.56	59.29	46.94	1,106,406	96.132
10	NN	Screening	67.74	70.38	73.65	72.47	59.54	46.73	1,101,575	96.131
11	NN	NLPQL	72.60	71.00	70.50	67.30	65.56	46.78	1,102,510	96.118
12	NN	MISQP	72.60	71.00	70.50	67.30	65.56	46.78	1,102,510	96.118
13	RS	MOGA	67.62	66.71	75.08	71.13	62.42	46.88	1,105,110	96.133
14	RS	Screening	68.04	68.04	74.89	73.13	64.36	46.76	1,102,109	96.130
15	RS	NLPQL	72.60	71.00	70.50	67.30	65.56	46.80	1,103,089	96.122
16	RS	MISQP	72.60	71.00	70.50	67.30	65.56	46.80	1,103,089	96.122

KR: Kriging; NPR: non-parametric regression; NN: neural network; RS: response surface; NLPQL: nonlinear programming by quadratic Lagrangian; MISQP: mixed-integer sequential quadratic programming; MOGA: multi-objective genetic algorithm.

Table 10. Multiple optimum candidates for the second optimization case (minimum cavitation, maximum efficiency and minimum aggregate objective function values are shown in bold fonts).

#	Metamodel	Optimizer	A1	A2	A3	A4	A5	Cavitation (Pa)	Head (m)	Shaft power (MW)	η (%)	AOF
1	KR	MOGA	-0.29	-3.43	-0.37	5.94	5.26	-65,239.24	44.14	1.041	96.190	-0.270
2	KR	Screening	-3.85	-0.77	2.97	4.62	6.06	-68,518.31	44.05	1.039	96.186	-0.233
3	NPR	MOGA	-4.26	-8.78	3.61	5.74	6.06	-64,078.42	44.03	1.039	96.186	-0.283
4	NPR	Screening	-2.53	-3.90	4.45	3.71	5.90	-67,624.60	44.01	1.038	96.177	-0.243
5	NN	MOGA	-6.01	-5.52	3.18	5.96	5.04	-66,458.48	44.20	1.043	96.174	-0.256
6	NN	Screening	3.32	-0.65	3.21	6.00	5.20	-67,110.62	44.07	1.037	96.179	-0.249
7	RS	MOGA	-6.97	-6.57	4.33	5.10	6.66	-63,789.31	44.03	1.038	96.182	-0.286
8	RS	Screening	0.18	-5.90	2.31	5.83	5.56	-65,690.41	44.01	1.038	96.187	-0.265

KR: Kriging; NPR: non-parametric regression; NN: neural network; RS: response surface; AOF: aggregate objective function; MOGA: multi-objective genetic algorithm.

where f_1 is the efficiency, f_{10} is the efficiency of the reference design, f_2 is the cavitation (the absolute value) and f_{20} is the cavitation (the absolute value) of the reference design. It is worthy here to note

that one may also choose to use the single objective maximum efficiency and single objective minimum cavitation (the absolute value) results for f_{10} and f_{20} , respectively.